





Experimental characterization of three-band braid relations in non-Hermitian acoustic lattices

Qicheng Zhang , Luekai Zhao, Xun Liu , Xiling Feng, Liwei Xiong, Wenquan Wu , and Chunyin Qiu *

Key Laboratory of Artificial Micro- and Nano-Structures of Ministry of Education
and School of Physics and Technology Wuhan University, Wuhan 430072, China



(Received 19 December 2022; accepted 19 April 2023; published 5 June 2023)

The nature of complex eigenenergy enables unique band topology in non-Hermitian (NH) lattices. Recently, there has been fast growing interest in the elusive winding and braiding topologies of the NH single and double bands, respectively. Here, we explore the even more intricate NH multiband topology and present an experimental characterization of the three-band braid relations by acoustic systems. Based on a concise tight-binding lattice model, we design a ternary cavity-tube structure equipped with a highly controllable unidirectional coupler, through which acoustic NH Bloch bands are experimentally reproduced in a synthetic space. We identify the NH braid relations from the global evolution of the eigenvalues and acoustic states, including a noncommutative braid relation $\sigma_1\sigma_2 \neq \sigma_2\sigma_1$ and a swappable braid relation $\sigma_1\sigma_2\sigma_1 = \sigma_2\sigma_1\sigma_2$. Our results could promote the understanding of NH Bloch band topology and pave the way toward designing practical devices for manipulating acoustic states.

DOI: [10.1103/PhysRevResearch.5.L022050](https://doi.org/10.1103/PhysRevResearch.5.L022050)

Introduction. Topological band theory, as one of the cornerstones in condensed matter physics, provides a unified framework for classifying distinct topological phases of matter [1,2]. Recently, the band topology in non-Hermitian (NH) lattices has attracted fast growing attention since it significantly broadens and deepens our understanding to the conventional Hermitian case [3–20]. Unlike the Hermitian band topology defined only by Bloch wave functions, the NH one can be defined either by Bloch or non-Bloch wave functions, because of the strikingly different energy spectra under periodic and open boundary conditions. This yields the Bloch or non-Bloch NH band theory. The former, still employing real-valued wave vectors and the conventional Brillouin zone (BZ), classifies the nontrivial topology of complex band structures [13–20], while the latter enables us to interpret unique open-boundary phenomena (e.g., skin effects) through introducing complex-valued wave vectors and a generalized BZ [3–12].

In the NH context, even a single Bloch band can be topologically nontrivial by generating complex-energy windings [21–24] and vortices [25,26]. While considering two Bloch bands, the systems can further exhibit rich braiding structures [2,27–29], which directly connect with the topology of encircling exceptional points (EPs) [2,30–36]. As for multiband systems, there are even more distinctive topological properties (e.g., noncommutative braid relations and associated nontrivial state permutations), since (i) they permit the

existence of multiple and higher-order EPs [37–41], and (ii) their homotopy group $B_N(N > 2)$ is non-Abelian [42–44]. Very recently, the appealing winding and braiding topologies have been demonstrated for single- and double-band systems by various experimental platforms [23,24,27–29]. However, experimental progress on multiband topology is still in its infancy [45]. Some recent experimental advances made for achieving acoustic non-Hermiticity could benefit the experimental implementation of this topic [24,29,46–49].

In this Letter, we report an experimental characterization of the NH three-band braid relations by acoustic systems. Theoretically, we propose a NH three-band lattice model, in which a series of band braids and state permutations are revealed from the topology of encircling multiple EPs. Experimentally, we employ the concept of synthetic dimension [23,27,49–53] to demonstrate the highly intricate three-band braiding physics inherited in one-dimensional (1D) NH Bloch bands, instead of using a large *finite* system where the truncated boundary drastically modifies the energy spectrum and eigenstates of the corresponding *infinite* lattice [2–5]. We consider a ternary-cavity structure equipped with a well-controlled unidirectional coupler. The latter, consisting of an external amplifier and a phase modulator, is elaborately designed to achieve the long-range, complex-valued, and momentum-resolved nonreciprocal couplings, which are extremely challenging in acoustics [29]. Typically, a noncommutative braid relation (NBR) and a swappable braid relation (SBR) are unambiguously captured not only by retrieving the complex band structures from the synthesized Hamiltonian, but also by directly observing the permutations of acoustic states. Our findings demonstrate the NH multiband topology in a fundamental manner that has no analog to the Hermitian one.

Three-band braid relations and lattice model. Here, we introduce the NH three-band braid relations governed by the

*Corresponding author: cyqiu@whu.edu.cn

Published by the American Physical Society under the terms of the [Creative Commons Attribution 4.0 International](https://creativecommons.org/licenses/by/4.0/) license. Further distribution of this work must maintain attribution to the author(s) and the published article's title, journal citation, and DOI.

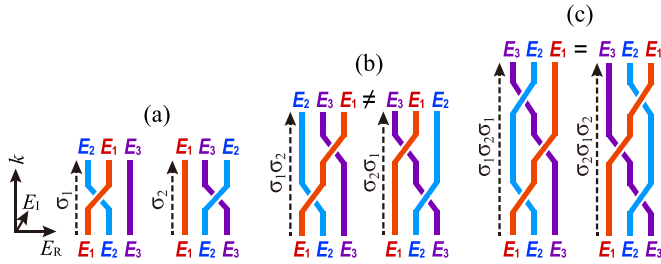


FIG. 1. Fundamental braid relations of NH three-band systems. The red, blue, and purple lines represent three separable complex energy bands braided in the (E_R, E_I, k) space. (a) Braid elements σ_1 and σ_2 . (b) Noncommutative braid relation (NBR) $\sigma_1\sigma_2 \neq \sigma_2\sigma_1$. (c) Swappable braid relation (SBR) $\sigma_1\sigma_2\sigma_1 = \sigma_2\sigma_1\sigma_2$.

braid group B_3 [42]. As depicted in Fig. 1, each band braid in the complex energy-momentum $(E-k)$ space is specified by a braid word, a product of the braid elements σ_1 and σ_2 . Specifically, σ_1 (σ_2) defines an anticlockwise braid where the first (second) band crosses over the second (third) band [Fig. 1(a)], resulting in an exchange of the eigenenergies E_1 (E_2) and E_2 (E_3). Note that the eigenenergies are sorted by their real parts. Intriguing braid relations arise when we alternately build up the band braids with σ_1 and σ_2 , as shown in Figs. 1(b) and 1(c). In terms of permuting eigenenergies, the braids $\sigma_1\sigma_2$ and $\sigma_2\sigma_1$ exhibit an inequivalent braiding consequence, i.e., $\sigma_1\sigma_2 \neq \sigma_2\sigma_1$ (dubbed NBR). More specifically, $\sigma_1\sigma_2$ gives rise to $[E_1, E_2, E_3] \rightarrow [E_2, E_3, E_1]$, whereas $\sigma_2\sigma_1$ results in $[E_1, E_2, E_3] \rightarrow [E_3, E_1, E_2]$. In contrast, the braids $\sigma_1\sigma_2\sigma_1$ and $\sigma_2\sigma_1\sigma_2$ present an equivalent braiding consequence despite that the two elements are exchanged, i.e., $\sigma_1\sigma_2\sigma_1 = \sigma_2\sigma_1\sigma_2$. We refer to it as the SBR. In this case, both $\sigma_1\sigma_2\sigma_1$ and $\sigma_2\sigma_1\sigma_2$ result in $[E_1, E_2, E_3] \rightarrow [E_3, E_2, E_1]$. Similar permutation properties are also exhibited in the global evolution of the eigenstates tied to the three *separable* NH bands.

All the above band braids can be realized in a simple three-band lattice model. As shown in Fig. 2(a), the orbitals 1, 2, and 3 (of zero on-site energy) are coupled by a reciprocal intracell hopping t_0 , and two nonreciprocal intercell hoppings t_m and t_n that span m and n lattices, respectively. The lattice Hamiltonian reads

$$\mathbf{H}(k) = \begin{pmatrix} 0 & t_0 & 0 \\ t_0 & 0 & t_0 \\ t_m e^{imk} + t_n e^{ink} & t_0 & 0 \end{pmatrix}. \quad (1)$$

To reflect the overall braiding degree of the three separable NH bands, we introduce an integer topological invariant v [27],

$$v := \sum_{i,j=1}^3 \frac{1}{2\pi i} \oint_{\text{BZ}} \frac{d \ln \tilde{E}_{ij}}{dk}, \quad (2)$$

where $\tilde{E}_{ij}(k) = [E_i(k) - E_j(k)]/2$ ($i \neq j$). Importantly, the nonreciprocal long-range couplings designed in our model ensure that all the braids are composed of the anticlockwise elements σ_1 and σ_2 , and hence the braiding degree v equals the total number of σ_1 and σ_2 (see the Supplemental Material (SM) [54]). This guides us to seek the desired braids from the phase diagram of v [Fig. 2(b)], where the dots label the parameters involved in our follow-up experiments. Note that the braid words, which are defined in an intact BZ $[k_0, k_0 + 2\pi]$, depend on the selection of the initial momentum k_0 ($-\pi/6$ throughout the work) [20].

As examples, Figs. 2(c) and 2(d) display two representative band braids, one for trivial (with $t_1 = 0.1$ and $t_2 = 0.3$) and the other for nontrivial (with $t_1 = 1.2$ and $t_2 = 0$), respectively. In the former case, the three bands do not braid with each other since the three complex eigenvalues E_1 , E_2 , and E_3 return to themselves trivially over the BZ. In the latter case, however, the eigenvalues permute and none of them come back to themselves, i.e., $[E_1, E_2, E_3] \rightarrow [E_2, E_3, E_1]$, a

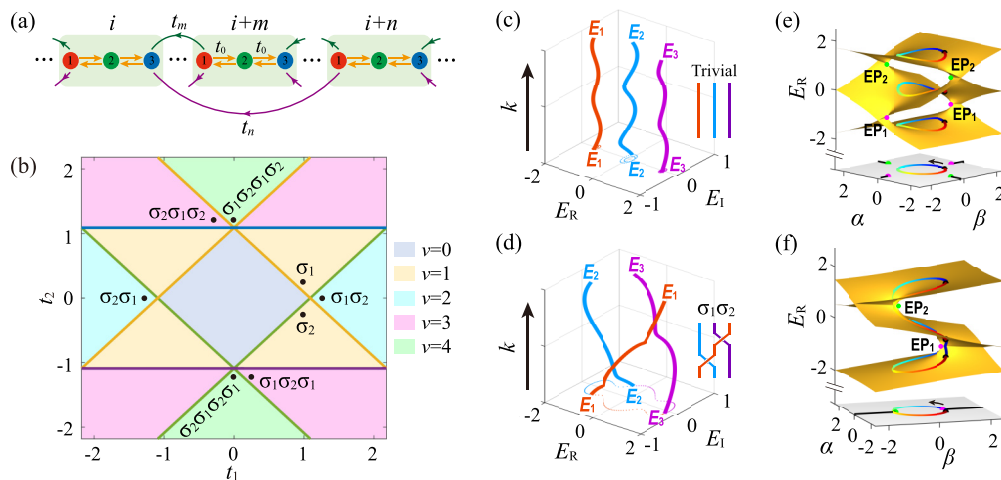


FIG. 2. One-dimensional NH lattice model and three-band braids. (a) A sketch of the three-band lattice model, where $t_0 = 1$, $t_m, t_n \in \mathbb{R}$, and $m, n > 0$ are assumed for simplicity. (b) Phase diagram exemplified for $m = 1$ and $n = 2$. The dots mark the band braids to be realized in our experiments. (c),(d) A trivial and a nontrivial three-band braids, respectively. (e),(f) The associated manifestations on Riemann surfaces (real parts), where EP_1 (EP_2) represents the EP formed by the lower (higher) two Riemann sheets. The eigenvalues, the EPs, and their branch cuts are projected to the $\alpha-\beta$ plane, on which the black dot is the starting point and the arrow indicates the evolution of the momentum.

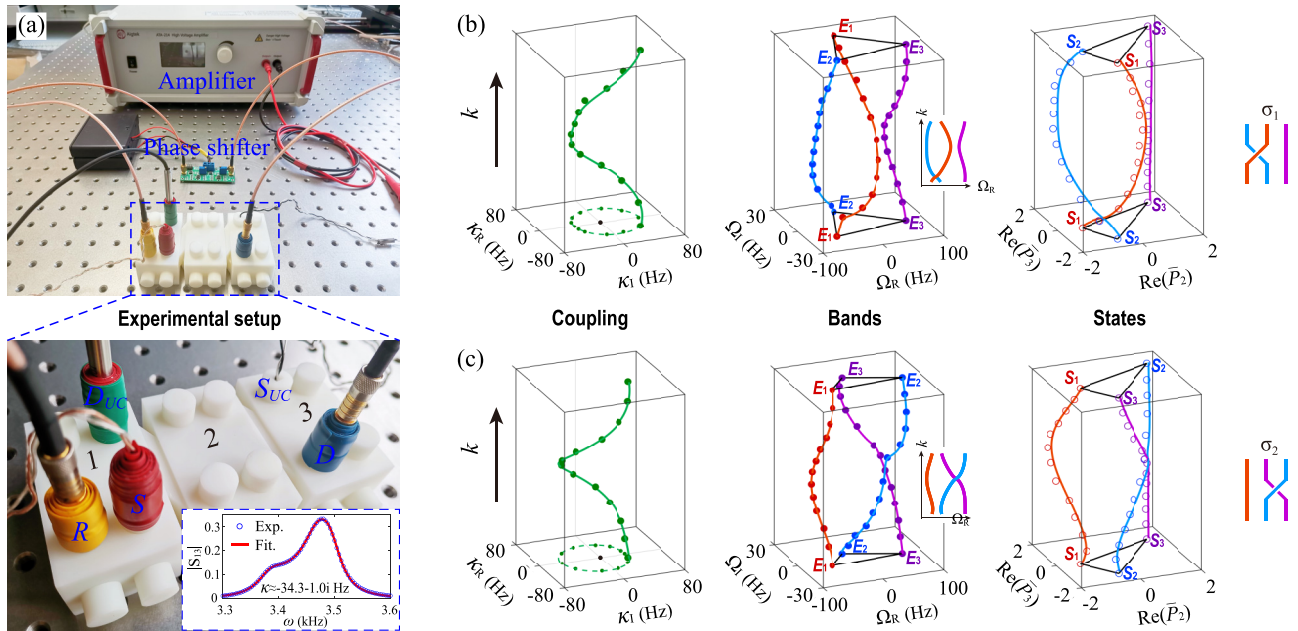


FIG. 3. Experimental setup and acoustic realization of the elementary braids σ_1 and σ_2 . (a) Experimental setup. The acoustic cavities 1, 2, and 3 emulate three orbitals and the narrow tubes in between mimic the reciprocal coupling t_0 . A controllable unidirectional coupler (UC), consisting of a microphone D_{UC} , an amplifier, a phase shifter, and a loudspeaker S_{UC} , is introduced between the cavities 1 and 3 to generate the unidirectional complex coupling $\kappa = \rho e^{i\theta}$. A source S and a detector D are used to excite and detect acoustic transmission responses, respectively, together with a detector R for phase reference. The inset exemplifies how the complex coupling κ is retrieved by fitting the transmission response $|S_{13}(\omega)|$. (b),(c) Experimental results for the elementary braids σ_1 and σ_2 , including the designed κ (left), the band braids (middle), and their projections on Ω_R - k plane (insets), and associated acoustic states (right). To facilitate observation, the initial and final eigenfrequencies (states) are linked into triangles. All experimental data (dots, circles) match well the theoretical predictions (lines).

manifestation of the Bloch band braid $\sigma_1\sigma_2$. The nontrivial eigenvalue permutation can be traced back to the underlying topology of encircling EPs on Riemann surfaces. To demonstrate that, we expand the k -space Hamiltonian $\mathbf{H}(k)$ into a parametric-space Hamiltonian $\mathbf{H}(\alpha, \beta)$ by the substitutions $\cos k \rightarrow \alpha$ and $\sin k \rightarrow \beta$, so that the BZ is mapped to a unit circle $\alpha^2 + \beta^2 = 1$ in (α, β) space. As shown in Figs. 2(e) and 2(f), the eigenvalues of $\mathbf{H}(\alpha, \beta)$ define three sheets of Riemann surfaces, and the eigenvalues of $\mathbf{H}(k)$ map out the colored loops on the sheets. When the loops do not encircle any EPs, the three eigenvalues of $\mathbf{H}(k)$ do not intersect and never exchange [Fig. 2(e)]. By contrast, encircling EPs inevitably cross the branch cuts of the Riemann surfaces, leading to a permutation of the eigenvalues. For instance, encircling EP₁ and EP₂ in sequence [Fig. 2(f)] results in the permutation process $[E_1, E_2, E_3] \rightarrow [E_2, E_1, E_3] \rightarrow [E_2, E_3, E_1]$, in accordance with the band braid $\sigma_1\sigma_2$ [Fig. 2(d)]. See more details in the SM [54]. Note that our NH three-band model with versatile EP topology is markedly different from the previous two-band models [2,20,27–29], in which the two-eigenvalue permutation turns out to be trivial in terms of non-Abelian effects.

Experimental characterization of the braid relations. Based on a concept of synthetic dimension, the above model can be implemented by designing an acoustic cavity-tube structure equipped with a unidirectional coupler (UC). As displayed in Fig. 3(a), the system consists of three identical air cavities with a complex dipole resonance frequency $\Omega_0 \approx 3450 - 24.4i$ Hz. The narrow tubes connecting two adjacent

cavities produce a reciprocal intracell coupling $t_0 \approx 43.3$ Hz. These intrinsic parameters are retrieved by fitting the transmission response $|S_{13}(\omega)|$ of the system in the absence of UC, where the subscripts i and j in $S_{ij}(\omega)$ denote the cavities inserted with the acoustic detector D and source S , respectively. On the other hand, a UC that consists of a microphone D_{UC} , an amplifier, a phase shifter, and a loudspeaker S_{UC} is introduced for achieving unidirectional coupling $\kappa = \rho e^{i\theta}$ between the cavities 1 and 3. Notice that the amplitude ρ and phase θ can be controlled by the amplifier and phase shifter, respectively [29]. Thus, we can use κ to mimic the *sole* k -dependent Hamiltonian element $\mathbf{H}_{31}(k) = t_m e^{imk} + t_n e^{ink}$, and reproduce the braiding physics of $\mathbf{H}(k)$ in the synthesized k space according to $\kappa = \mathbf{H}_{31}(k)$. Turning on the UC and using the already assessed intrinsic parameters, the value of κ can be precisely retrieved by fitting the transmission response $|S_{13}(\omega)|$, as exemplified in the inset of Fig. 3(a). Eventually, we obtain the complex band structures by substituting all the fitted parameters into $\mathbf{H}(k)$ and solving the k -resolved eigenfrequencies $\Omega = \Omega_R + i\Omega_I$.

Figures 3(b) and 3(c) show our experimental results for the two elementary band braids σ_1 and σ_2 . First, we tune the UC to ensure the unidirectional coupling $\kappa(k) \approx 1.0t_0 e^{ik} + 0.2t_0 e^{i2k}$, at a momentum step of $\pi/6$ [Fig. 3(b), left]. In the 3D space spanned by (Ω_R, Ω_I, k) , the red and blue bands twist around each other, and the purple band stays out of the twist [Fig. 3(b), middle]. (For clarity, Ω_0 is deducted from the complex eigenfrequency Ω .) As a visual manifestation of the band braid σ_1 , the eigenfrequencies E_1 and E_2 permute

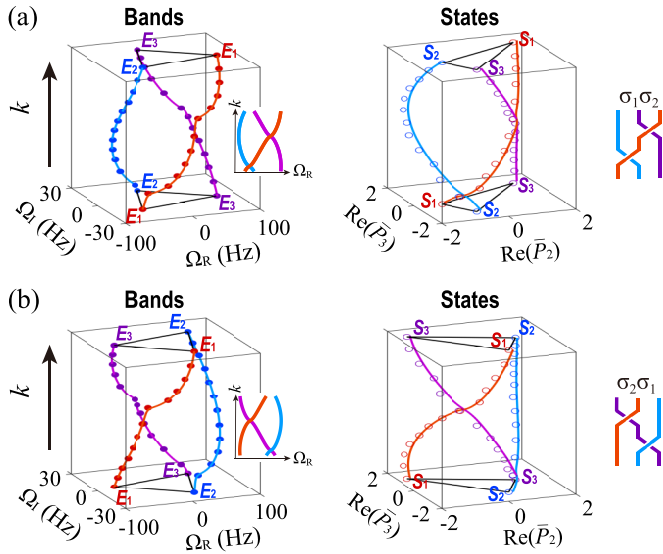


FIG. 4. Experimental characterization of the NBR $\sigma_1\sigma_2 \neq \sigma_2\sigma_1$. The results of the band braids $\sigma_1\sigma_2$ (a) and $\sigma_2\sigma_1$ (b) indicate inequivalent braiding consequences in both the eigenvalues (left) and acoustic states (right).

as k evolves over the BZ. Similarly, the band braid σ_2 is realized by tuning $\kappa(k) \approx 1.0t_0e^{ik} - 0.2t_0e^{i2k}$. As expected, the retrieved band structure [Fig. 3(c), middle] exhibits a clearly permutation between E_2 and E_3 . It is worth pointing out that the eigenfrequency permutations are closely related to the global evolution of acoustic states in the synthetic k space, since essentially the nonreciprocal coupling and the resultant effective Hamiltonian are directly retrieved from real acoustic signals. To demonstrate this more clearly, we further measure the acoustic responses $P_1 = S_{13}(\Omega_R)$, $P_2 = S_{23}(\Omega_R)$, and $P_3 = S_{33}(\Omega_R)$, and extract their real-part information $[1, \text{Re}\bar{P}_2, \text{Re}\bar{P}_3]^T$ with $\bar{P}_2 = P_2/P_1$ and $\bar{P}_3 = P_3/P_1$. The results are presented in the right panels of Figs. 3(b) and 3(c). It is shown that the acoustic states exhibit consistent permutation behaviors with those of eigenfrequencies, i.e., $[S_1, S_2, S_3] \rightarrow [S_2, S_1, S_3]$ for σ_1 and $[S_1, S_2, S_3] \rightarrow [S_1, S_3, S_2]$ for σ_2 .

Now we experimentally characterize the NBR through controlling $\kappa(k)$ to map the phase points $(t_1, t_2) = (1.2, 0)$ and $(t_1, t_2) = (-1.2, 0)$ (see the SM [54]). Their braid words can be recognized respectively as $\sigma_1\sigma_2$ [Fig. 4(a)] and $\sigma_2\sigma_1$ [Fig. 4(b)] via the projected band structures (insets). Under the braid $\sigma_1\sigma_2$, the eigenfrequencies change from $[E_1, E_2, E_3]$ into $[E_2, E_3, E_1]$, and the corresponding acoustic states permute from $[S_1, S_2, S_3]$ to $[S_2, S_3, S_1]$. The braid $\sigma_2\sigma_1$, however, undergoes an entirely different permutation process, $[E_1, E_2, E_3] \rightarrow [E_3, E_1, E_2]$ and $[S_1, S_2, S_3] \rightarrow [S_3, S_1, S_2]$. These phenomena directly witness the inequivalent (or non-Abelian) braiding consequences of $\sigma_1\sigma_2$ and $\sigma_2\sigma_1$. Different from the non-Abelian characteristics unveiled for three NH states evolving in real space [58–60] or parametric space [61,62], here we aim to the braiding topology in momentum space, which is of great significance for understanding the fundamental Bloch band theory for NH lattice systems. Note that both the braids $\sigma_1\sigma_2$ and $\sigma_2\sigma_1$ have an even permutation parity associated to the global biorthogonal Berry

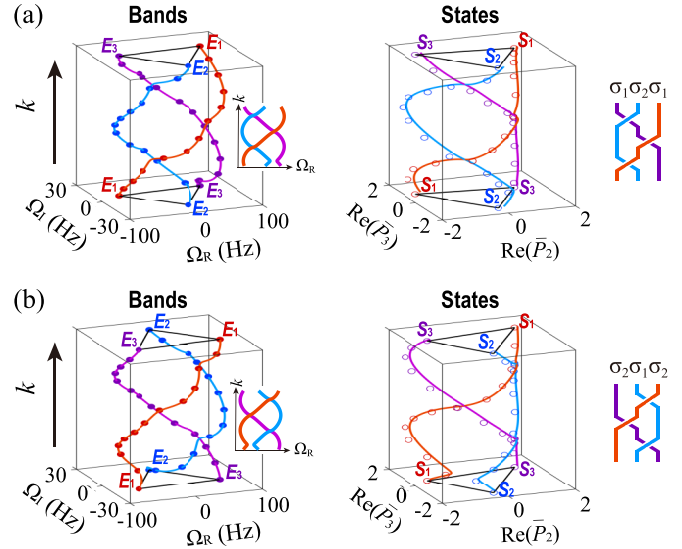


FIG. 5. Experimental characterization of the SBR $\sigma_1\sigma_2\sigma_1 = \sigma_2\sigma_1\sigma_2$. The results of the band braids $\sigma_1\sigma_2\sigma_1$ (a) and $\sigma_2\sigma_1\sigma_2$ (b) identify equivalent braiding consequences in both the eigenvalues (left) and acoustic states (right).

phase $Q = 0$ [20]. However, their inequivalent braiding consequences are still characterized by the unequal non-Abelian Berry phases [63], which can be explicitly described by the unitary matrices $[0 \ 1 \ 0; 0 \ 0 \ 1; 1 \ 0 \ 0]$ and $[0 \ 0 \ 1; 1 \ 0 \ 0; 0 \ 1 \ 0]$, respectively.

Figure 5 shows our experimental results for characterizing the SBR $\sigma_1\sigma_2\sigma_1 = \sigma_2\sigma_1\sigma_2$. To reproduce such band braids, we tune $\kappa(k)$ to map the phase points $(t_1, t_2) = (0.3, -1.2)$ and $(t_1, t_2) = (-0.3, 1.2)$ [54]. As predicted, the three acoustic bands twist in a more intricate way, which form two band braids with swapped elements, i.e., $\sigma_1\sigma_2\sigma_1$ [Fig. 5(a)] and $\sigma_2\sigma_1\sigma_2$ [Fig. 5(b)], respectively. More importantly, these braids exhibit equivalent braiding consequences in terms of permuting eigenvalues and eigenstates: $[E_1, E_2, E_3] \rightarrow [E_3, E_2, E_1]$ and $[S_1, S_2, S_3] \rightarrow [S_3, S_2, S_1]$. In addition, the two braids have the same global biorthogonal Berry phase $Q = \pi$ and non-Abelian Berry phase $[0 \ 0 \ 1; 0 \ 1 \ 0; 1 \ 0 \ 0]$. The former indicates the same odd permutation parity, while the latter evidences the equivalence in braiding consequence.

Conclusions and discussion. From both the perspectives of eigenfrequencies and acoustic states, we have evidenced the two fundamental braid relations for the highly intricate NH three-band braiding topology. We have not only demonstrated a variety of NH acoustic braids in synthetic dimension, but also achieved all possible permutation consequences for the three-state braiding systems. Our experimental results indicate that an input acoustic state can be manipulated into any of the six output states by designing complex band structures, which could advance the applications on acoustic logic gates and switches.

The braid relations can be further generalized for any two equilength but distinct braid sequences consisting of σ_1 and σ_2 alternatively. That is, if the total number of the braiding elements is a multiple of 3, their braiding consequences are

equivalent; otherwise inequivalent (see the SM [54] for the proof). The latter has been experimentally evidenced by the braids $\sigma_1\sigma_2\sigma_1\sigma_2$ and $\sigma_2\sigma_1\sigma_2\sigma_1$ emerging in Fig. 2(b) [54]. In future, our experiments could also be extended to demonstrate the collective behaviors (e.g., creation, split, braiding, annihilation, coalescence, etc.) of multiple (or higher-order) EPs and associated band topologies [41,44], the band braiding

topologies in two and higher dimensions [39–41], and the interplays between the band braiding and non-Hermitian skin effects/topological edge states [7,13,17,22].

Acknowledgments. This work was supported by the National Natural Science Foundation of China (Grants No. 11890701 and No. 12104346), and the Young Top-Notch Talent for Ten Thousand Talent Program (2019-2022).

-
- [1] A. Bansil, H. Lin, and T. Das, Colloquium: Topological band theory, *Rev. Mod. Phys.* **88**, 021004 (2016).
- [2] H. Shen, B. Zhen, and L. Fu, Topological Band Theory for Non-Hermitian Hamiltonians, *Phys. Rev. Lett.* **120**, 146402 (2018).
- [3] S. Yao and Z. Wang, Edge States and Topological Invariants of Non-Hermitian Systems, *Phys. Rev. Lett.* **121**, 086803 (2018).
- [4] F. K. Kunst, E. Edvardsson, J. C. Budich, and E. J. Bergholtz, Biorthogonal Bulk-Boundary Correspondence in Non-Hermitian Systems, *Phys. Rev. Lett.* **121**, 026808 (2018).
- [5] K. Yokomizo and S. Murakami, Non-Bloch Band Theory of Non-Hermitian Systems, *Phys. Rev. Lett.* **123**, 066404 (2019).
- [6] K. Kawabata, N. Okuma, and M. Sato, Non-Bloch band theory of non-Hermitian Hamiltonians in the symplectic class, *Phys. Rev. B* **101**, 195147 (2020).
- [7] N. Okuma, K. Kawabata, K. Shiozaki, and M. Sato, Topological Origin of Non-Hermitian Skin Effects, *Phys. Rev. Lett.* **124**, 086801 (2020).
- [8] E. J. Bergholtz, J. C. Budich, and F. K. Kunst, Exceptional topology of non-Hermitian systems, *Rev. Mod. Phys.* **93**, 015005 (2021).
- [9] L. Xiao, T. Deng, K. Wang, G. Zhu, Z. Wang, W. Yi, and P. Xue, Non-Hermitian bulk–boundary correspondence in quantum dynamics, *Nat. Phys.* **16**, 761 (2020).
- [10] T. Helbig, T. Hofmann, S. Imhof, M. Abdelghany, T. Kiessling, L. W. Molenkamp, C. H. Lee, A. Szameit, M. Greiter, and R. Thomale, Generalized bulk–boundary correspondence in non-Hermitian topoelectrical circuits, *Nat. Phys.* **16**, 747 (2020).
- [11] X. Zhang, Y. Tian, J.-H. Jiang, M.-H. Lu, and Y.-F. Chen, Observation of higher-order non-Hermitian skin effect, *Nat. Commun.* **12**, 5377 (2021).
- [12] W. Wang, X. Wang, and G. Ma, Non-Hermitian morphing of topological modes, *Nature (London)* **608**, 50 (2022).
- [13] K. Kawabata, K. Shiozaki, M. Ueda, and M. Sato, Symmetry and Topology in Non-Hermitian Physics, *Phys. Rev. X* **9**, 041015 (2019).
- [14] D. S. Borgnia, A. J. Kruchkov, and R.-J. Slager, Non-Hermitian Boundary Modes and Topology, *Phys. Rev. Lett.* **124**, 056802 (2020).
- [15] J. Zhong, K. Wang, Y. Park, V. Asadchy, C. C. Wojcik, A. Dutt, and S. Fan, Nontrivial point-gap topology and non-Hermitian skin effect in photonic crystals, *Phys. Rev. B* **104**, 125416 (2021).
- [16] R. Okugawa, R. Takahashi, and K. Yokomizo, Non-Hermitian band topology with generalized inversion symmetry, *Phys. Rev. B* **103**, 205205 (2021).
- [17] K. Zhang, Z. Yang, and C. Fang, Correspondence between Winding Numbers and Skin Modes in Non-Hermitian Systems, *Phys. Rev. Lett.* **125**, 126402 (2020).
- [18] C. C. Wojcik, X.-Q. Sun, T. Bzdušek, and S. Fan, Homotopy characterization of non-Hermitian Hamiltonians, *Phys. Rev. B* **101**, 205417 (2020).
- [19] Z. Li and R. S. K. Mong, Homotopical characterization of non-Hermitian band structures, *Phys. Rev. B* **103**, 155129 (2021).
- [20] H. Hu and E. Zhao, Knots and Non-Hermitian Bloch Bands, *Phys. Rev. Lett.* **126**, 010401 (2021).
- [21] N. Hatano and D. R. Nelson, Localization Transitions in Non-Hermitian Quantum Mechanics, *Phys. Rev. Lett.* **77**, 570 (1996).
- [22] Z. Gong, Y. Ashida, K. Kawabata, K. Takasan, S. Higashikawa, and M. Ueda, Topological Phases of Non-Hermitian Systems, *Phys. Rev. X* **8**, 031079 (2018).
- [23] K. Wang, A. Dutt, K. Y. Yang, C. C. Wojcik, J. Vučković, and S. Fan, Generating arbitrary topological windings of a non-Hermitian band, *Science* **371**, 1240 (2021).
- [24] L. Zhang, Y. Yang, Y. Ge, Y. J. Guan, Q. Chen, Q. Yan, F. Chen, R. Xi, Y. Li, D. Jia, S. Q. Yuan, H. X. Sun, H. Chen, and B. Zhang, Acoustic non-Hermitian skin effect from twisted winding topology, *Nat. Commun.* **12**, 6297 (2021).
- [25] N. Hatano and D. R. Nelson, Vortex pinning and non-Hermitian quantum mechanics, *Phys. Rev. B* **56**, 8651 (1997).
- [26] K. Kim and D. R. Nelson, Interaction effects in non-Hermitian models of vortex physics, *Phys. Rev. B* **64**, 054508 (2001).
- [27] K. Wang, A. Dutt, C. C. Wojcik, and S. Fan, Topological complex-energy braiding of non-Hermitian bands, *Nature (London)* **598**, 59 (2021).
- [28] Y. Yu, L.-W. Yu, W. Zhang, H. Zhang, X. Ouyang, Y. Liu, D.-L. Deng, and L.-M. Duan, Experimental unsupervised learning of non-Hermitian knotted phases with solid-state spins, *npj Quantum Inf.* **8**, 116 (2022).
- [29] Q. Zhang, Y. Li, H. Sun, X. Liu, L. Zhao, X. Feng, X. Fan, and C. Qiu, Observation of Acoustic Non-Hermitian Bloch Braids and Associated Topological Phase Transitions, *Phys. Rev. Lett.* **130**, 017201 (2023).
- [30] M. V. Berry, Physics of nonhermitian degeneracies, *Czech. J. Phys.* **54**, 1039 (2004).
- [31] W. D. Heiss, The physics of exceptional points, *J. Phys. A: Math. Theor.* **45**, 444016 (2012).
- [32] Q. Zhong, M. Khajavikhan, D. N. Christodoulides, and R. El-Ganainy, Winding around non-Hermitian singularities, *Nat. Commun.* **9**, 4808 (2018).
- [33] K. Kawabata, T. Bessho, and M. Sato, Classification of Exceptional Points and Non-Hermitian Topological Semimetals, *Phys. Rev. Lett.* **123**, 066405 (2019).
- [34] J. Feilhauer, A. Schumer, J. Doppler, A. A. Mailybaev, J. Bohm, U. Kuhl, Moiseyev N, and S. Rotter, Encircling

- exceptional points as a non-Hermitian extension of rapid adiabatic passage, *Phys. Rev. A* **102**, 040201(R) (2020).
- [35] K. Ding, C. Fang, and G. Ma, Non-Hermitian topology and exceptional-point geometries, *Nat. Rev. Phys.* **4**, 745 (2022).
- [36] S. Sayyad, M. Stalhammar, L. Rodland, and F. K. Kunst, Symmetry-protected exceptional and nodal points in non-Hermitian systems, [arXiv:2204.13945](https://arxiv.org/abs/2204.13945).
- [37] Z. Yang, A. P. Schnyder, J. Hu, and C.-K. Chiu, Fermion Doubling Theorems in Two-Dimensional Non-Hermitian Systems for Fermi Points and Exceptional Points, *Phys. Rev. Lett.* **126**, 086401 (2021).
- [38] I. Mandal and E. J. Bergholtz, Symmetry and Higher-Order Exceptional Points, *Phys. Rev. Lett.* **127**, 186601 (2021).
- [39] H. Hu, S. Sun, and S. Chen, Knot topology of exceptional point and non-Hermitian no-go theorem, *Phys. Rev. Res.* **4**, L022064 (2022).
- [40] C. C. Wojcik, K. Wang, A. Dutt, J. Zhong, and S. Fan, Eigenvalue topology of non-Hermitian band structures in two and three dimensions, *Phys. Rev. B* **106**, L161401 (2022).
- [41] J. L. K. König, K. Yang, J. C. Budich, and E. J. Bergholtz, Braid protected topological band structures with unpaired exceptional points, [arXiv:2211.05788](https://arxiv.org/abs/2211.05788).
- [42] C. Kassel and V. Turaev, *Braid Groups* (Springer, New York, 2008).
- [43] E. J. Pap, D. Boer, and H. Waalkens, Non-Abelian nature of systems with multiple exceptional points, *Phys. Rev. A* **98**, 023818 (2018).
- [44] C.-X. Guo, S. Chen, K. Ding, and H. Hu, Exceptional Non-Abelian Topology in Multiband Non-Hermitian Systems, *Phys. Rev. Lett.* **130**, 157201 (2023).
- [45] Z. Li, K. Ding, and G. Ma, Eigenvalue knots and their isotopic equivalence in three-state non-Hermitian systems, *Phys. Rev. Res.* **5**, 023038 (2023).
- [46] R. Fleury, D. Sounas, and A. Alù, An invisible acoustic sensor based on parity-time symmetry, *Nat. Commun.* **6**, 5905 (2015).
- [47] C. Shi, M. Dubois, Y. Chen, L. Cheng, H. Ramezani, Y. Wang, and X. Zhang, Accessing the exceptional points of parity-timesymmetric acoustics, *Nat. Commun.* **7**, 11110 (2016).
- [48] H.-X. Li, M. Rasendo-Lopez, Y.-F. Zhu, X.-D. Fan, D. Torrent, B. Liang, J.-C. Cheng, and J. Christensen, Ultrathin acoustic parity-time symmetric metasurface cloak, *Research* **2019**, 8345683 (2019).
- [49] J.-J. Liu, Z.-W. Li, Z.-G. Chen, W. Tang, A. Chen, B. Liang, G. Ma, and J.-C. Cheng, Experimental Realization of Weyl Exceptional Rings in a Synthetic Three-Dimensional Non-Hermitian Phononic Crystal, *Phys. Rev. Lett.* **129**, 084301 (2022).
- [50] L. Yuan, Q. Lin, M. Xiao, and S. Fan, Synthetic dimension in photonics, *Optica* **5**, 1396 (2018).
- [51] M. Lohse, C. Schweizer, H. M. Price, O. Zilberberg, and I. Bloch, Exploring 4D quantum Hall physics with a 2D topological charge pump, *Nature (London)* **553**, 55 (2018).
- [52] E. Lustig, S. Weimann, Y. Plotnik, Y. Lumer, M. A. Bandres, A. Szameit, and M. Segev, Photonic topological insulators in synthetic dimensions, *Nature (London)* **567**, 356 (2019).
- [53] A. Dutt, Q. Lin, L. Yuan, M. Minkov, M. Xiao, and S. Fan, A single photonic cavity with two independent physical synthetic dimensions, *Science* **367**, 59 (2020).
- [54] See Supplemental Material at <http://link.aps.org/supplemental/10.1103/PhysRevResearch.5.L022050> for more theoretical, numerical, and experimental details, which includes Refs. [20,42,55–57].
- [55] A. A. Soluyanov and D. Vanderbilt, Smooth gauge for the topological insulators, *Phys. Rev. B* **85**, 115415 (2012).
- [56] H. A. Haus, *Waves and Fields in Optoelectronics* (Prentice-Hall, Englewood Cliffs, NJ, 1984).
- [57] S. Wonjoo, W. Zheng, and F. Shanhuai, Temporal coupled-mode theory and the presence of non-orthogonal modes in lossless multimode cavities, *IEEE J. Quantum Electron.* **40**, 1511 (2004).
- [58] Z.-G. Chen, R.-Y. Zhang, C. T. Chan, and G. Ma, Classical non-Abelian braiding of acoustic modes, *Nat. Phys.* **18**, 179 (2021).
- [59] O. You, S. Liang, B. Xie, W. Gao, W. Ye, J. Zhu, and S. Zhang, Observation of Non-Abelian Thouless Pump, *Phys. Rev. Lett.* **128**, 244302 (2022).
- [60] X.-L. Zhang, F. Yu, Z.-G. Chen, Z.-N. Tian, Q.-D. Chen, H.-B. Sun, and G. Ma, Non-Abelian braiding on photonic chips, *Nat. Photon.* **16**, 390 (2022).
- [61] Y. S. S. Patil, J. Höller, P. A. Henry, C. Guria, Y. Zhang, L. Jiang, N. Kralj, N. Read, and J. G. E. Harris, Measuring the knot of non-Hermitian degeneracies and non-commuting braids, *Nature (London)* **607**, 271 (2022).
- [62] W. Tang, K. Ding, and G. Ma, Experimental realization of non-Abelian permutations in a three-state non-Hermitian system, *Nat. Sci. Rev.* **9**, nwac010 (2022).
- [63] D. Vanderbilt, *Berry Phases in Electronic Structure Theory: Electric Polarization, Orbital Magnetization and Topological Insulators* (Cambridge University Press, Cambridge, England, 2018).